Published in final edited form as:
Immunity. 2010 November 24; 33(5): 713–722. doi:10.1016/j.immuni.2010.11.010.

microRNAs prevent the generation of autoreactive antibodies

Laura Belver, **Virginia G de Yébenes**, and **Almudena R Ramiro**
DNA Hypermutation and Cancer Group. Spanish National Cancer Research Center (CNIO), Madrid 28029, Spain

SUMMARY

MicroRNAs have been shown critical for a number of aspects of immune system regulation and function. Here we have examined the role of microRNAs in terminal B cell differentiation by analysing *Cd19*-Cre$^{ki/+}$ Dicer$^{fl/fl}$ mice. We found that in the absence of Dicer the transitional and marginal zone (MZ) B cell compartments are overrepresented, and follicular (FO) B cell generation is impaired. microRNA analysis reveals that miR185, a microRNA overexpressed in FO cells, dampens BCR signalling through Btk downregulation. Dicer deficient B cells have a skewed BCR repertoire with hallmarks of autoreactivity, which correlates with high titers of autoreactive antibodies in serum and autoimmune features in females. Together, our results reveal a crucial role of microRNAs in late B cell differentiation and in the establishment of B cell tolerance.

INTRODUCTION

Primary antibody diversification is generated during B cell differentiation in the bone marrow through somatic DNA rearrangement of immunoglobulin (Ig) genes by V(D)J recombination (Bassing et al., 2002). Due to its stochastic nature, antibody diversification can give rise to B cell antigen receptors (BCR) that recognize the body's self components and potentially lead to autoimmunity. This pathological outcome is usually prevented by tolerance mechanisms which are governed by signals delivered by the BCR (Gu et al., 1991; Hartley et al., 1991; Meffre et al., 2000; Meffre and Wardemann, 2008; Shlomchik, 2008; Wardemann and Nussenzweig, 2007). Two main checkpoints ensure B cell tolerance; one is established in the bone marrow in early immature B cells that have completed V(D)J recombination of heavy and light Ig genes (Goodnow et al., 1988; Nemazee and Burki, 1989; Wardemann et al., 2003), the second takes place in peripheral B cells in transit to their final maturation (Wardemann et al., 2003). At this late maturation stage transitional B cells can give rise to two functionally distinct peripheral populations: follicular (FO) or marginal zone (MZ) B cells (Allman and Pillai, 2008; Carsetti et al., 2004). FO versus MZ fate decision is functionally coupled to BCR signalling (Carsetti et al., 2004; Pillai and Cariappa, 2009) and it has been suggested that B cells bearing BCRs with autoreactive specificities are preferentially driven into a MZ fate (Li et al., 2002; Martin and Kearney, 2000). However, the molecular mechanisms that regulate this transition and its link to B cell tolerance establishment remain poorly understood.

MicroRNAs are small RNA (21-22 nucleotides long) post-transcriptional regulators of gene expression, which have been unveiled critical for numerous aspects of the regulation and maintenance of the mammalian immune system (Martinez and Busslinger, 2007; Xiao and Rajewsky, 2009). Mature microRNAs are generated through the sequential cleavage of longer RNA precursors by Drosha and Dicer RNA endonuclases (Kim et al., 2009). Early

Corresponding author: Almudena R Ramiro aramiro@cnio.es Phone No. 0034 917328000-3510 Fax No. 0034 917328033.

Europe PMC Funders Author Manuscripts

Dicer ablation in the B cell lineage results in an almost complete block of B cell differentiation at the pro-B cell stage, due to an aberrant regulation of apoptosis in the bone marrow (Koralov et al., 2008). These results highlight the essential role of microRNAs in B cell generation in the bone marrow; however the severity of the phenotype precluded the analysis of terminal B cell differentiation and selection.

Here we have addressed the role of microRNAs at late B cell differentiation stages in *Cd19*-Cre$^{ki/+}$Dicer$^{fl/fl}$ mice. Mature B cells are generated in *Cd19*-Cre$^{ki/+}$Dicer$^{fl/fl}$ mice, where transitional and MZ B cells are overrepresented and the generation of FO B cells is impaired. microRNA analysis revealed that miR185, a microRNA differentially expressed in FO versus MZ B cells, promotes downregulation of the BCR signalling effector Bruton Tyrosine Kinase (Btk) in activated B cells. Importantly, Dicer deficient B cells produce high titers of autoreactive antibodies, which correlate with the presence of autoimmune features in aged female animals. Therefore our results provide evidence for a role of microRNAs in terminal B cell differentiation and in the establishment of B cell tolerance.

RESULTS

Mature B cells are generated in *Cd19*-Cre$^{ki/+}$Dicer$^{fl/fl}$ mice

To address the function of microRNAs at late stages of B cell development we generated B cell specific Dicer deficient mice by breeding *Cd19*-Cre$^{ki/+}$ (Rickert et al., 1997) to Dicer$^{fl/fl}$ mice (Harfe et al., 2005). *Cd19*-Cre-mediated deletion takes place gradually during bone marrow differentiation (Hobeika et al., 2006; Schmidt-Supprian and Rajewsky, 2007). In contrast, Dicer ablation by mb1-Cre (Koralov et al., 2008) promoted deletion of close to 100% of bone marrow B lineage cells (Hobeika et al., 2006) from the pro-B cell stage (Koralov et al., 2008). Consistently, *Cd19*-Cre$^{ki/+}$Dicer$^{fl/fl}$ mice showed a significant depletion (86% reduction) of Dicer mRNA in immature B220^{+}IgM^{+} bone marrow cells but not at earlier differentiation stages (Fig. S1a). Analysis of bone marrow revealed a mild reduction of total B220^{+} cells in *Cd19*-Cre$^{ki/+}$Dicer$^{fl/fl}$ mice (Fig. 1a) although percentages of pro-B, pre-B and immature IgM^{+} cells were normal (Fig. S1b-c and Fig. 1b). In contrast, the proportion of recirculating IgD^{+} cells was reduced in *Cd19*-Cre$^{ki/+}$Dicer$^{fl/fl}$ mice to 35% of control levels (19,7+/−10,0% vs 7,0+/−4,8%) (Fig. 1b), suggesting that the reduced number of B220^{+} cells in Dicer deficient bone marrow is mostly accounted for by a defect in the generation of mature B cells, rather than in earlier stages. In agreement with these results, the percentage of peripheral B cells was reduced in spleen and lymph nodes in *Cd19*-Cre$^{ki/+}$Dicer$^{fl/fl}$ mice (spleen, 50,2+/−7.2% *vs* 35,0+/−7,5%; lymph nodes 14,7+/−5,6% *vs* 6,0+/−2,3%, Fig. 1c-d), with absolute spleen B cell numbers reduced to 41% of those in control animals (Fig. S1d and Table S1). Non-B cell subsets, including T regulatory cells, were present in normal numbers and showed normal levels of Dicer expression in *Cd19*-Cre$^{ki/+}$Dicer$^{fl/fl}$mice (Fig. S1d-i), indicating that Dicer is specifically depleted in the B cell lineage in this model. No differences were observed when *Cd19*-Cre$^{ki/+}$Dicer$^{fl/+}$ mice were compared to *Cd19*-Cre$^{ki/+}$Dicer$^{+/+}$ mice (data not shown). Therefore, Dicer depletion in *Cd19*-Cre$^{ki/+}$Dicer$^{fl/fl}$ mice is compatible with the generation of peripheral B cells but their number is severely reduced.

Peripheral B cell subsets are shifted in *Cd19*-Cre$^{ki/+}$Dicer$^{fl/fl}$ mice

Once in the periphery, transitional IgM^{+} B cells progressively start expressing IgD and terminally differentiate into either marginal zone (MZ) or follicular (FO) B cells (Carsetti et al., 2004; Su et al., 2004). FO or conventional B cells (CD21^{+}CD23^{bright}CD93$^{−}$) populate the inner follicle and are associated to T-dependent immune responses. In contrast, MZ B cells (CD21^{bright}CD23^{+}) are recruited to the outer layer of spleen follicles and provide a first and rapid response against blood-borne antigens (Martin et al., 2001). In addition, a third B

cell subset, called B1 cells, populates the spleen and peritoneal cavities and is believed to contribute with natural antibodies to T-independent responses (Allman and Pillai, 2008; Martin et al., 2001). Both MZ and B1 cells have been associated with the generation of self-reactive antibodies (Allman and Pillai, 2008; Dammers et al., 2000; Hayakawa et al., 1984; Li et al., 2002; Martin and Kearney, 2000). We found that in *Cd19*-Cre$^{ki/+}$Dicer$^{fl/fl}$ mice the percentage of spleen transitional B cells (CD21^{+}CD23^{bright}CD93^{+}) is increased (39,8+/−12,8% *vs* 16+/−7,3%), and the percentage of FO B cells (CD21^{+}CD23^{bright}CD93^{-}) is decreased (24,1+/−8,6% *vs* 60,4+/− 3,2%) (Fig.1e-f). This effect is accompanied by an overrepresentation of MZ B cells (10,8+/−4,8% vs 20,8+/−6,2%) (Fig. 1e and Table S1) and of B1a and B1b subsets (Fig. S1j-k). These results suggest that the absence of Dicer preferentially drives differentiation of transitional B cells into MZ B cells rather than FO B cells.

Terminal differentiation of transitional cells is altered in Dicer deficient mice

The relative contribution of different spleen B cell subsets reflects a severe drop in the absolute number of FO cells while transitional and MZ B cell numbers are normal or slightly increased (Table S1). A number of mouse models with defective B cell differentiation tend to accumulate a higher proportion of MZ and B1 cells accompanying a severe defect of FO cell generation (Martin and Kearney, 2002). This phenomenon is probably due to complex homeostatic mechanisms that seemingly compensate a lymphopenic scenario by favouring the generation of a competent first-barrier defence provided by B1 and MZ cells (reviewed in (Martin and Kearney, 2002). To discriminate whether the MZ versus FO bias observed in Dicer deficient animals is due to lymphopenia-driven compensatory events or to a true requirement of microRNAs for FO B cell differentiation from transitional cells, we performed reconstitution experiments using bone marrow mixed chimeras. We mixed wild type CD45.1^{+} bone marrow cells with CD45.2^{+} cells from either *Cd19*-Cre$^{ki/+}$Dicer$^{fl/+}$ (50% Dicer$^{fl/+}$) or *Cd19*-Cre$^{ki/+}$Dicer$^{fl/fl}$ (50% Dicer$^{fl/fl}$) mice. Unmixed bone marrow cells from CD45.2^{+} *Cd19*-Cre$^{ki/+}$Dicer$^{fl/+}$ (100% Dicer$^{fl/+}$) and *Cd19*-Cre$^{ki/+}$Dicer$^{fl/fl}$ (100% Dicer$^{fl/fl}$) mice were used as controls. Cells were transferred into lethally irradiated CD45.2^{+} wild type hosts and bone marrow and spleen reconstitution was assessed after 12 weeks. At this timepoint, the number of CD45.2^{+} B220^{+} cells was <1% of normal levels in mice that were transferred with CD45.1 cells alone, indicating that the contribution of host-derived B cell progenitors is negligible in these experiments (not shown). As expected, we found that 100% Dicer$^{fl/fl}$ reconstitution resulted in a decrease of both IgD^{+} bone marrow and FO spleen subsets as compared to 100% Dicer$^{fl/+}$ reconstituted mice, phenocopying our observations in *Cd19*-Cre$^{ki/+}$Dicer$^{fl/+}$ and *Cd19*-Cre$^{ki/+}$Dicer$^{fl/fl}$ animals (Fig. 2a). CD45.1^{+} wild type cells alleviate the lymphopenia driven by Dicer deficient cells, as 50% Dicer$^{fl/fl}$ mixed chimeras contain total absolute numbers of transitional, FO and MZ cells indistinguishable from those in 50% Dicer$^{fl/+}$ control chimeras (Table S2). In spite of this normal numbers of total spleen cells, we observed that CD45.2^{+} cells in 50% Dicer$^{fl/fl}$ reconstituted mice still show an impairment of FO B cell generation (60.6+/−3.5% *vs* 34.9+/−2.6%) and an overrepresentation of the MZ compartment (8.7+/−1.5% *vs* 13.8+/−2.7%) (Fig. 2b and Table S2). These results indicate that MZ overrepresentation in Dicer deficient animals is not a homeostatic response secondary to lymphopenia, but instead reflects a skewed terminal differentiation pattern promoted by the absence of microRNAs. To rule out that this phenotype could be the result of an enhanced depletion of microRNAs taking place specifically in FO cells, we measured Dicer levels in transitional, MZ and FO cells from CD19-Cre$^{ki/+}$Dicer$^{fl/+}$ and CD19-Cre$^{ki/+}$Dicer$^{fl/fl}$ spleens (Fig. S2). This analysis showed that Dicer levels are lowest at the transitional stage of CD19-Cre$^{ki/+}$Dicer$^{fl/fl}$ spleens and that they slightly increase in mature FO cells. This result indicates that Dicer depletion does not proceed beyond the transitional stage and rather suggests that those cells retaining some Dicer expression selectively differentiate into FO cells. We conclude that Dicer depletion in

late B cell differentiation results in a biased terminal differentiation of transitional cells that impairs FO cell development while favouring the generation of MZ cells.

microRNA profiling in FO and MZ B cells

To probe the microRNAs that could be functionally relevant in determining the FO versus MZ B cell fate, we performed microarray analysis and compared microRNA expression in FO and MZ B cells from CD19-Cre$^{ki/+}$Dicer$^{fl/+}$ mice. FO and MZ B cells where isolated by cell sorting and RNA was labelled and hybridized to microRNA arrays. We consistently detected expression of 177 microRNAs in FO cell samples. Statistical analysis was performed to identify those microRNAs that are differentially expressed in MZ *vs* FO B cells ($p<0,1$, see Methods section). This analysis showed that 31 of the 177 detected microRNAs are differentially expressed in these two subsets (Fig. 3a), all of which were found to be expressed at lower levels in FO CD19-Cre$^{ki/+}$Dicer$^{fl/fl}$ than in FO CD19-Cre$^{ki/+}$Dicer$^{fl/+}$ cells (not shown), as expected from the absence of Dicer. Interestingly, we found that in CD19-Cre$^{ki/+}$Dicer$^{fl/+}$ control animals all 31 microRNAs are expressed at higher levels in FO than in MZ B cells (Fig. 3a). This result was validated by real-time RT-PCR for a number of microRNAs, including miR141, miR16, miR192 and miR194. In all the cases we found that RT-PCR results confirmed that these microRNAs display higher expression levels in FO than in MZ B cells (Fig. S3a). This observation accords with our finding that in CD19-Cre$^{ki/+}$Dicer$^{fl/fl}$ mice MZ generation is favoured over FO generation and suggests that microRNAs can be more determinant for FO than MZ B cell differentiation.

miR185 and Btk deregulation in CD19-Cre$^{ki/+}$Dicer$^{fl/fl}$ B cells results in a shifted response to BCR stimulation

To gain insights into the functional relevance of the differentially expressed microRNAs identified by array analysis, we followed a hypothesis-driven bioinformatics approach by searching for microRNAs that could target genes reported to play a role in the FO *vs* MZ B cell generation. In particular, we performed a prediction search using three independent softwares (MiRanda, miRBase and TargetScan) by scanning all differentially expressed microRNAs for potential binding to Aiolos, Btk, CD21 and Notch2. We found that all three softwares predict miR185 to target one such gene, *Btk* (Fig. S3b), with an identical seed sequence at position 17-39 of its 3′UTR. Btk, a kinase that transduces signals downstream of the BCR, has been shown to be involved in the generation or recruitment of autoreactive B cells to the MZ area (Martin and Kearney, 2000). Real-time PCR analysis confirmed that miR185 expression is regulated in peripheral B cell subsets, with transitional cells displaying intermediate miR185 levels that are upregulated in FO cells and downregulated in MZ cells (Fig. S3c).To test if miR185 can be regulating *Btk* expression in B cells, we overexpressed miR185 in primary B cells from wild type spleens and measured *Btk* expression by real-time PCR after 3 days of LPS+IL4 stimulation. We found that miR185 transduction, but not transduction of mock or an irrelevant miRNA (miR27a) vector, results in a decrease of *Btk* mRNA levels (Fig. 3b, $p=0.005$). Dicer expression itself, included as a control, is unchanged in B cells transduced with either three vectors (Fig. 3b). Importantly, we found that Btk protein levels are increased in CD19-Cre$^{ki/+}$Dicer$^{fl/fl}$ spleen B cells when compared to CD19-Cre$^{ki/+}$Dicer$^{fl/+}$ counterparts (Fig. 3c). Specifically, Btk levels are significantly increased in transitional and FO CD19-Cre$^{ki/+}$Dicer$^{fl/fl}$ cells, while this difference is not evident in MZ cells, in agreement with the observed block in FO but not MZ B cell differentiation (Fig. 3d). The strength of BCR signalling is critical to determine B cell fate (Grimaldi et al., 2005; Pillai and Cariappa, 2009; Shlomchik, 2008) and *Btk* has been reported as one of the components involved in establishing this threshold and to influence the differentiation of MZ B cells (Halcomb et al., 2008; Khan et al., 1995; Martin and Kearney, 2000; Ng et al., 2004; Satterthwaite et al., 1997). To determine whether

Europe PMC Funders Author Manuscripts

elevated Btk levels correlate with enhanced BCR signalling in CD19-Cre$^{ki/+}$Dicer$^{fl/fl}$ B cells, we examined the increase of ERK phosphorylation in CD19-Cre$^{ki/+}$Dicer$^{fl/+}$ and CD19-Cre$^{ki/+}$Dicer$^{fl/fl}$ B cells in response to BCR stimulation. We found that stimulation with anti-IgM antibodies consistently results in a higher level of ERK phosphorylation in Dicer deficient B cells when compared to control cells (Fig. 3e). We next addressed downstream events of BCR signalling by analysing the efficiency of class switch recombination in B cells stimulated with anti-IgM and IL4. Consistently with the observed increase in Btk protein levels and ERK phosphorylation, CD19-Cre$^{ki/+}$Dicer$^{fl/fl}$ B cells show a higher rate of class switch recombination to IgG1 (1.5+/−0.25% versus 3.2+/−0.78% at 72 hours, p=0.03) (Fig. 3f). To address if deregulated levels of miR185 and Btk are directly responsible for the enhanced BCR signalling phenotype, we performed gain-of-function experiments. Spleen B cells from wild type mice were BCR stimulated with anti-IgM and IL-4, transduced with retroviruses encoding either Btk or miR185 precursor and the rate of class switch recombination to IgG1 was measured. We found that Btk overexpression recapitulates the phenotype observed in CD19-Cre$^{ki/+}$Dicer$^{fl/fl}$ B cells, i.e. increases the rate of class switch recombination (control, 5.3+/−1.6%; Btk-transduced, 7.7+/−2.1%). Conversely, miR185 overexpression results in a decrease of the class switch recombination efficiency (control, 5.3+/−1.6%; miR185-transduced, 4.0+/−1.8%) (Fig. 3g). Together, these results establish a direct role of miR185 downregulation in the modulation of BCR signalling in CD19-Cre$^{ki/+}$Dicer$^{fl/fl}$ B cells through the release of negative regulation of Btk and suggest that altered BCR signalling is responsible for the biased selection and commitment of CD19-Cre$^{ki/+}$Dicer$^{fl/fl}$ peripheral B cells.

CD19-Cre$^{ki/+}$Dicer$^{fl/fl}$ B cells express a skewed Ig repertoire

To determine whether the altered pattern of B cell generation and BCR signalling results in a skewed selection of the antibody repertoire in the absence of microRNAs, we examined the VDJ rearrangements of the expressed immunoglobulin heavy chains in B cells from CD19-Cre$^{ki/+}$Dicer$^{fl/+}$ and CD19-Cre$^{ki/+}$Dicer$^{fl/fl}$ mice. Spleen B cells were isolated and the proportion of J_H elements was determined after RT-PCR, cloning, sequencing and Ig Blast analysis (Table S3, Fig. 4a). We found that the usage of J_H genes was significantly altered (p=0.0002) in CD19-Cre$^{ki/+}$Dicer$^{fl/fl}$ as compared to control B cells, with an overrepresentation of J_H4 segments in Dicer deficient cells (Fig. 4a). In addition, the number of R and K residues at the CDR3 region, a feature of autoreactivity (Crouzier et al., 1995; Ichiyoshi and Casali, 1994; Wardemann et al., 2003), was significantly increased in CD19-Cre$^{ki/+}$Dicer$^{fl/fl}$ B cells (Fig. 4b). Therefore, in the absence of Dicer there is a redistribution of variable segments in the antibody repertoire.

CD19-Cre$^{ki/+}$Dicer$^{fl/fl}$ females display autoimmune features

The observation that microRNA deficient B cells contain a higher number of positive charges in their Ig heavy chains prompted us to assess the autoreactivity of serum Igs from CD19-Cre$^{ki/+}$Dicer$^{fl/+}$ and CD19-Cre$^{ki/+}$Dicer$^{fl/fl}$ mice. Sera from CD19-Cre$^{ki/+}$Dicer$^{fl/+}$ and CD19-Cre$^{ki/+}$Dicer$^{fl/fl}$ animals was collected and antibody reactivity against self-antigens was measured by ELISA and compared to titers found in MRL$^{lpr/lpr}$ mice. Importantly, we found that titers of IgGs against dsDNA, ssDNA and cardiolipin autoantigens are significantly increased in serum from aged female but not male CD19-Cre$^{ki/+}$Dicer$^{fl/fl}$ mice (Fig. 5a-c). Although total IgG and IgM antibody titers are on average slightly increased in CD19-Cre$^{ki/+}$Dicer$^{fl/fl}$ mice (not shown), this difference is not statistically significant and does not correlate with the autoantibody titers in individual mice (Fig.S4). This suggests that accumulation of autoantibodies in the absence of Dicer is not passively correlated to higher total Ig titers, but rather the result of a biased repertoire selection. To address the pathogenity of autoantibodies in Dicer deficient females we assessed the presence of immune complexes in kidney sections. Indeed, immunoflurescence analysis revealed a

prominent accumulation of IgG in CD19-Cre$^{ki/+}$Dicer$^{fl/fl}$ aged females when compared to control animals (Fig. 6a and Fig. S5a), indicative of deposition of immune complexes. Moreover, silver-PAS staining of kidney sections revealed massive lymphocyte infiltration and overall damage of glomerulus architecture that affected 50% of aged Dicer deficient females (Fig. 6b and Fig. S5b). We conclude that the absence of microRNAs gives rise to a skewed antibody repertoire enriched in self-reactive specificities that leads to the development of autoimmune disease.

DISCUSSION

In this study we have addressed the role of microRNAs in terminal B cell differentiation by analysing CD19-Cre$^{ki/+}$Dicer$^{fl/fl}$ mice. Although CD19 expression and Dicer deletion could be expected to take place at the pre-B stage of bone marrow development (Rickert et al., 1997), we found that the level of Dicer mRNA is significantly decreased only in bone marrow IgM^{+} cells. This late depletion, which probably reflects a gradual deletion during bone marrow differentiation (Hobeika et al, 2006) together with a high stability of Dicer mRNA, allowed the generation of mature B cells and their migration to peripheral tissues. Indeed, the sharpest reduction in Dicer levels was observed in spleen transitional cells. We found here that in the absence of Dicer, normal numbers of transitional B cells are generated, which can differentiate normally into MZ B cells; in contrast, the generation of FO B cells is severely compromised. Interestingly, this biased differentiation is cell autonomous, which indicates that microRNAs are critical for MZ versus FO cell fate determination. In this regard, we provide in this study the first analysis of microRNA expression in MZ versus FO B cells. Notably, we found that only a relatively reduced number of microRNAs are differentially expressed in MZ *vs* FO cells, all of which display a higher expression level in the latter population. This global overexpression of microRNAs in the FO subset could in turn be related to the higher level of Dicer expression found in FO cells as compared with transitional or MZ B cells (Fig S2). Differential Dicer expression in these B cell subsets is a somehow unexpected result that deserves further investigation. Regardless of the regulatory mechanism responsible for this expression pattern, this microRNA profiling can open new perspectives on the study of the developmental program that determines the selective mechanisms operating at transitional B cells and their final commitment into MZ and FO subsets.

Therefore, a number of evidences presented here support the idea that FO B cell generation has a deeper dependency on microRNA expression: i) Dicer deficient B cell progenitors give rise to normal numbers of transitional and MZ cells but to severely reduced numbers of FO cells, as measured in CD19-Cre$^{ki/+}$Dicer$^{fl/fl}$ animals, bone marrow transfers and competitive bone marrow chimeras, ii) in wild type animals, differentially expressed microRNAs show higher expression levels in FO than in MZ and iii) the few FO cells that are generated in CD19-Cre$^{ki/+}$Dicer$^{fl/fl}$ mice express higher Dicer levels than their immediate precursors –transitional cells-, suggesting that only cells where Dicer depletion is incomplete –i.e. deletion of a single allele-selectively differentiate into the FO lineage.

Btk is known to influence the MZ versus FO lineage decision and we report here that miR185 negatively regulates the expression of Btk in primary B cells. We show that miR185 expression is regulated during terminal B cell differentiation, with intermediate levels at the transitional stage that become downregulated in MZ B cells and upregulated in FO cells. Importantly, this expression pattern mirrors the levels of Btk expression, which suggests that higher Btk levels are more compatible with the generation of MZ B cells, and a link between the skewed generation of MZ and FO cells observed in Dicer deficient animals and an altered BCR signalling. We provide evidence that this is indeed the case. Dicer deficient B cells contain higher levels of Btk protein and ERK phosphorylation and they undergo class

switch recombination in response to BCR stimulation at a higher rate than control animals. This effect is phenocopied by Btk overexpression and counterbalanced by miR185 overexpression. Therefore, although other molecular pathways can play a role in the observed phenotype in CD19-Cre$^{ki/+}$Dicer$^{fl/fl}$ mice, our data provide evidence that miR185 and Btk contribute to determining B cell fate by influencing the outcome of BCR signalling.

This notion is further reinforced by the finding that the Ig repertoire expressed by peripheral B cells is skewed in these animals. This observation could be explained by a shifted usage of J_H segments during V(D)J recombination or by an abnormal selection of the Ig repertoire. However, as major Dicer mRNA depletion is first observed in immature IgM$^+$ cells, the first possibility is very unlikely and our results rather support the view that in Dicer deficient B cells the establishment of tolerance is incomplete. Our data suggest that Dicer deficiency results in lower levels of miR185 and accumulation of Btk, which in turn can allow the selection of B cells bearing self-reactive BCRs and favour the final commitment of some of these cells into a MZ fate. This hypothesis is compatible with the observation that relatively subtle changes in Btk expression and/or activity influence the generation of MZ and FO cells (Dingjan et al., 1998; Maas et al., 1999) and could explain the observed accumulation of serum autoantibodies and the presence of features of autoimmune disease in aged Dicer deficient animals.

Interestingly, the autoimmune disease observed in Dicer deficient animals was predominantly found in female rather than male mice, very much resembling the profound prevalence of female incidence in various autoimmune diseases in humans, such as systemic lupus erythematosus, Sjoegren's syndrome or scleroderma (Whitacre, 2001). Therefore, we envision that the analysis of microRNA expression profiles can prove clinically useful in the diagnosis and prognosis of autoimmune disease. In summary, our data provide evidence on the role of microRNAs in maintaining a tolerant antibody repertoire and will contribute a new perspective on gender-biased autoimmune syndromes by allowing the study of microRNA-based gene regulation under differential hormone contexts.

METHODS

Mice

B cell specific Dicer deficient (CD19-Cre$^{ki/+}$Dicer$^{fl/fl}$) and littermate control (CD19-Cre$^{ki/+}$Dicer$^{fl/+}$) mice were generated by breeding Dicer$^{fl/fl}$ to CD19-Cre$^{ki/+}$ (Harfe et al., 2005; Rickert et al., 1997) mice. All mice were housed under pathogen-free conditions in accordance with the recommendations of the Federation of European Laboratory Animal Science Associations. All experiments were performed following the Animal Bioethics and Comfort Committee protocols approved by the Instituto de Salud Carlos III.

Flow cytometry

Cells from bone marrow and spleen were collected and erythrocytes were lysed with ACK Lysing Buffer (BioWhittaker). Then cells were cell-surface stained with different combinations of anti-mouse Btk, IgM, IgD, IgG1, Mac-1, CD3, CD4, CD5, CD21, CD23, CD25, CD43 and CD45.2 (BD Biosciences), anti-B220 (Miltenyi Biotec) and anti-CD93 (eBioscience) antibodies. For Btk intracellular staining, extracellular marked cells were fixed with PFA and permeabilized with 0.05% saponin and stained with anti-Btk antibody in 1X PBS – 0.05% saponin. Flow cytometry analyses were performed in a FACSCanto flow cytometer using FACSDiva (BD Biosciences) or FlowJo (Tree Star) softwares.

Bone marrow reconstitution

5 ×10^6 total bone marrow cells from CD45.1 C57BL/6, CD45.2 CD19-$Cre^{ki/+}$$Dicer^{fl/+}$ or CD45.2 CD19-$Cre^{ki/+}$$Dicer^{fl/fl}$ donor mice were injected intravenously into 8- to 12-week-old CD45.2 C57BL/6 mice that had been lethally irradiated (2 × 550 cGy) 24h before the reconstitution. For competitive bone marrow reconstitutions, mice were injected with cell mixtures containing 2.5 ×10^6 bone marrow cells from CD45.1 C57BL/6 mice and 2.5 ×10^6 bone marrow cells from CD45.2 CD19-$Cre^{ki/+}$$Dicer^{fl/+}$ or CD19-$Cre^{ki/+}$$Dicer^{fl/fl}$ mice. Chimeric mice were analyzed 12 weeks after the reconstitution.

Cell cultures

293T cells were cultured in DMEM supplemented with 10% FCS. Primary spleen B cells were purified from spleens by immunomagnetic depletion with anti-CD43 beads (Miltenyi Biotec) and cultured in RPMI 1640 supplemented with 10% FCS, 10 mM Hepes (Invitrogen), 50 μM β-mercaptoethanol (Invitrogen). For Btk expression analysis upon miRNA overexpression, 25 μg/mL LPS (Sigma-Aldrich) and 10 ng/mL IL4 (PeproTech) were added to the medium. For class switch recombination analysis, 10 μg/mL F(ab)'$_2$ fragments of goat anti-mouse IgM (Jackson Immunoresearch) and 10 ng/mL IL4 (PeproTech) were added to the medium.

Retroviral infection

Retroviral supernatants were produced by transient calcium phosphate cotransfection of NIH-293T cells with pCL-Eco (Imgenex) and pre-miRNA-GFP retroviral vectors or pMXPIE-Btk retroviral vector. pre-miRNA-GFP vectors encoded pre-miRNA (pre-miR27a or pre-miR185) and their flanking 50bp-long genomic sequences(de Yebenes et al., 2008). Mouse primary B cells were transduced with retroviral supernatants for 20 hours in the presence of 8 μg/ml polybrene (Sigma), 10 mM Hepes (Invitrogen) and 50 μM β-mercaptoethanol (Invitrogen). For Btk expression analysis upon miRNA overexpression, 25μg/ml LPS (Sigma) and 10ng/ml IL-4 (Peprotech) were added to the retroviral supernatants. GFP positive cells were sorted 48 hours post-transduction (FACSAria, BD Biosciences). For class switch recombination analysis upon Btk or miR185 overexpression, 10 μg/mL F(ab)'$_2$ fragments of goat anti-mouse IgM (Jackson Immunoreserach) and 10 ng/mL IL4 (PeproTech) were added to the retroviral supernatant. 96 hours after transduction IgG1 expression in GFP positive cells was determined by flow cytometry.

miRNA microarrays

Spleens cells from CD19-$Cre^{ki/+}$$Dicer^{fl/+}$ and CD19-$Cre^{ki/+}$$Dicer^{fl/fl}$ mice were stained with anti-B220, anti-CD21 and anti-CD23 antibodies as described above. $B220^+CD21^{bright}CD23^+$ (marginal zone) and $B220^+CD21^+CD23^{bright}$ (follicular) B cell populations were sorted (FACSAria, BD Biosciences) and total RNA of purified populations was extracted with TRIzol (Invitrogen) following manufacturer's instructions. miRNA microarray hybridations were performed on Mouse miRNA Microarray platform (Agilent Technologies). Local background was subtracted from median signal and intensity was transformed to a $\log_2$ scale. Normalized data were analyzed with MultiExperiment Viewer software. First, paired t test was used to determine differentially expressed miRNAs in MZ *vs* FO control (CD19-$Cre^{ki/+}$$Dicer^{fl/+}$) cells. miRNAs with a p-value ≤ 0.1 and fold expression difference ≥ 2 were selected for further analysis. Then control (CD19-$Cre^{ki/+}$$Dicer^{fl/+}$) and Dicer deficient (CD19-$Cre^{ki/+}$$Dicer^{fl/fl}$) cells were compared using an unpaired t test for both MZ and FO subsets. Again, miRNAs with a p-value ≤ 0.1 and fold expression difference ≥ 2 were selected. 31 miRNAs were identified in FO – control *vs* Dicer deficient analysis and only 4 in MZ – control *vs* Dicer deficient analysis, all of which were contained in the FO analysis results.

Real-time PCR

B cell populations were sorted from spleen or bone marrow after staining with B220, IgM, CD21, CD23 and CD93 antibodies. T regulatory cells were isolated (>90% purity) using the CD4+CD25+ Regulatory T cell Isolation Kit (Miltenyi Biotec). Total RNA was extracted with TRIzol (Invitrogen) and converted into cDNA using random hexamers (Roche) and SuperScript II reverse transcriptase (Invitrogen). Mouse Dicer and Btk mRNA were quantified using SYBR green assay (Applied Biosystems). GAPDH amplifications were used as normalization controls. The following primers were used: Dicer (forward): 5′ – ACGAAATGCAAGGAATGGACTC – 3′ Dicer (reverse): 5′ – GGCACCAGCAAGAGACTCAAA – 3′ Btk (forward): 5′ – AGCGCTCCCAGCAGAAAAA – 3′ Btk (reverse): 5′ – TCTTACTGCCTCTTCTCCCACG – 3′ GAPDH (forward): 5′ – TGAAGCAGGCATCTGAGGG – 3′ GAPDH (reverse): 5′ – CGAAGGTGGAAGAGTGGGAG – 3′ For mature miRNA expression analysis, total RNA was extracted as previously described. Retrotranscription and real time PCR were performed using TaqMan MicroRNA Assays (Applied Biosystems) following the recommendations of the manufacturer. Amplification of sno142 was used as a normalization control.

Western blotting

Spleen B cells from CD19-Cre$^{ki/+}$Dicer$^{fl/+}$ and CD19-Cre$^{ki/+}$Dicer$^{fl/fl}$ mice were purified by immunomagnetic depletion as described above. For Btk western blot, cell pellets were incubated on ice for 20 minutes in lysis buffer containing 20mM Tris, 150mM NaCl, 1% Nonidet P-40 in the presence of protease inhibitors (Roche) and lysates were cleared by centrifugation. For phospho-ERK and ERK western blot, cells were incubated for 1 hour at 37°C in starvation buffer (RPMI 1640, 10 mM Hepes, 50μM β-mercaptoethanol) prior to stimulation with 10 μg/mL F(ab)'$_2$ fragments of goat anti-mouse IgM (Jackson Immunoreserach). Cells were pelleted after the indicated times and lysed on ice for 30 minutes in lysis buffer containing 50mM Tris-HCl pH 7.4, 1% Nonidet P-40, 137.5mM NaCl and 1% glycerol in the presence of protease inhibitors (Roche) and phosphatase inhibitors (NaV and NaF). Lysates were cleared by centrifugation at 4°C for 15 minutes at 16000 × g and 5% β-mercaptoethanol was added.

Total protein was sized-fractioned by SDS-PAGE on 10% acrylamide-bisacrylamide gel and transferred to Protran nitrocellulose membrane (Whatman) in transfer buffer (0.19 M glycine, 25 mM Tris base, 0.01% SDS) containing 20% methanol. Gels were transferred for 1 hour at 0.4A for Btk and 2 hours at 0.2A for phospho-ERK / ERK western blot. Membranes were probed with anti-mouse-Btk (Abcam) and anti-mouse-Tubulin (Sigma-Aldrich) and anti-mouse-phospho-ERK (Cell Signalling) and anti-mouse-ERK (Biosource) primary antibodies respectively. Then membranes were incubated with corresponding secondary HRP-conjugated antibodies (Dako) and developed using SuperSignal West Dura Extended Duration Substrate (Thermo Scientific).

Amplification and analysis of V(D)J rearrangments

Spleen B cells from CD19-Cre$^{ki/+}$Dicer$^{fl/+}$ and CD19-Cre$^{ki/+}$Dicer$^{fl/fl}$ mice were purified and total RNA was extracted and converted into cDNA as described above. IgH rearrangments were amplified from RT-PCR products using 2.5 U of Taq DNA polymerase (Roche) and combining a 3′ primer for Cμ exon 1 with a 5′ primer for V_H7183 or V_HJ558. Amplification consisted of 30 cycles (30" at 94°C, 30" at 57°C, 60" at 72°C) followed by a 10 minutes incubation at 72°C. PCR products were cloned into the pGEM-T Easy vector (Promega). Clones were selected randomly and sequenced using T7 universal primer. Sequences were analyzed using NCBI IgBlast program (http://www.ncbi.nlm.nih.gov/igblast/). Cμ: 5′ – ATTTGGGAAGGACTGACTCT – 3′ V_H7183: 5′ –

GAGTCTGGGGGAGCTTA – 3′ V_HJ558: 5′ – RGCCTGGGRCTTCAGTGAAG – 3′ (R = A or G)

ELISA

Quantification of IgG and IgM autoantibodies recognizing DNA and cardiolipin was performed by ELISA. For anti-DNA antibodies quantification, MaxiSorp Immuno plates (Nunc) were incubated with 50 μg/mL poly-L-lysine (Sigma-Aldrich) for 2 hours at 37°C, then rinsed with water and coated with 100 μL of 2 μg/mL calf thymus DNA (Sigma-Aldrich) in phosphate buffered saline (1X PBS, 0.14 M NaCl, 0.01 M NaH_2PO_4) at 4°C overnight. Single-stranded DNA was obtained by boiling DNA for 10 minutes and snap-chilling on ice. For anti-cardiolipin detection, plates were coated with 100 μL of 20 μg/mL cardiolipin in ethanol at 4°C overnight. Coated plates were blocked with 4% BSA PBS for 90 minutes at RT and wash with 0.05% Tween 20 in PBS. Sera were diluted in 1% BSA PBS, 1:500 for IgG anti-DNA antibodies and 1:100 for IgM anti-DNA and IgG anti-cardiolipin antibodies detection. 50 μL of the dilutions were applied and incubated for 2 hours at RT. Plates were washed again and autoantibodies were detected using anti – mouse - κ/λ – chains – POD – conjugates (Mouse IgG ELISA Kit, Roche) or goat anti-mouse IgM HRP conjugated antibody (Bethyl laboratories) followed by SuperSignal ELISA Femto Maximum Sensitivity Substrate (Thermo Scientific). The OD425nm was determined using a conventional microplate reader. Serum from $MRL^{lpr/lpr}$ and RAG2 knock-out mice were used as positive and negative controls respectively. The relative binding capacity to DNA or cardiolipin was calculated by subtracting background signal from RAG2 knock-out serum and normalizing to $MRL^{lpr/lpr}$ signal. For determination of serum total Ig titers, Mouse IgG ELISA Kit (Roche) and Mouse IgM ELISA Quantitation Kit (Bethyl laboratoires) were used following manufacturer's instructions.

Immunofluorescence

Kidneys were embedded on OCT compound (Tissue Tek, Sakura) and snap-frozen on dry ice. 10 μm sections were cut and fixed in chilled acetone for 10 minutes. Sections were washed with PBS, blocked for 30 minutes with blocking buffer (PBS, 1% BSA, 0.3% Triton, 0.5% goat serum, 0.5% donkey serum, 1% gelatin), stained with Alexa Fluor 488 donkey anti-mouse IgG (Invitrogen) and analyzed in a Leica TCS-SP5 (AOBS) confocal microscope with a 20X HC PL APO 0.7 N.A. oil immersion objective using LAS AF software. Background was substracted from mean fluoresce intensity of each glomerulus and obtained values were normalized to control mean.

Histopathology

Kidneys were fixed in 10% buffered formalin and embedded in paraffin. Sections were stained with Silver methenamine P.A.S.M. according to standard protocols.

Statistical analysis

Bone marrow, spleen and lymph nodes phenotypes, relative Dicer and Btk mRNA and protein expression and glomerulus fluorescence intensities were analyzed with Student's t-tests. Sequence analyses were performed with 2-tailed Chi-square tests. For autoantibody ELISAs, a threshold was established for each particular antigen (mean of CD19-$Cre^{ki/+}Dicer^{fl/+}$ mice serum signals plus two standard deviations). Sera with signals above this threshold were considered autoreactive and Fisher's exact test was performed. For renal damage measurement, the number of affected glomeruli was analyzed using Fisher's exact test. Statistical analyses were carried out using GraphPad software. The level of statistical significance was preset at $p < 0.05$.

Europe PMC Funders Author Manuscripts

Supplementary Material

Refer to Web version on PubMed Central for supplementary material.

Acknowledgments

We would like to thank Dr CJ Tabin and Dr K Rajewsky for kindly providing us with Dicer$^{fl/fl}$ and CD19-Cre$^{Ki/+}$ mice, respectively, Drs V Barreto, O Fernandez-Capetillo, I Moreno de Alborán and T Wossning for critical reading of the manuscript and Drs JM Ligos, S Minguet, M Cañamero, DG Pisano, D Megías, O Domínguez, D Martínez and C Velasco for technical advice.

LB is supported by the Spanish National Cancer Research Center (CNIO), VGY is a Ramón y Cajal Investigator (Ministerio de Ciencia e Innovación) and ARR is funded by CNIO. This work was funded by grants from Ministerio de Ciencia e Innovación (SAF2007-63130), Comunidad Autónoma de Madrid (DIFHEMAT-CM) and European Research Council Starting Grant program (BCLYM-207844).

REFERENCES

Allman D, Pillai S. Peripheral B cell subsets. Curr Opin Immunol. 2008; 20:149–157. [PubMed: 18434123]

Bassing CH, Swat W, Alt FW. The mechanism and regulation of chromosomal V(D)J recombination. Cell. 2002; 109(Suppl):S45–55. [PubMed: 11983152]

Carsetti R, Rosado MM, Wardmann H. Peripheral development of B cells in mouse and man. Immunol Rev. 2004; 197:179–191. [PubMed: 14962195]

Crouzier R, Martin T, Pasquali JL. Heavy chain variable region, light chain variable region, and heavy chain CDR3 influences on the mono- and polyreactivity and on the affinity of human monoclonal rheumatoid factors. J Immunol. 1995; 154:4526–4535. [PubMed: 7722307]

Dammers PM, Visser A, Popa ER, Nieuwenhuis P, Kroese FG. Most marginal zone B cells in rat express germline encoded Ig VH genes and are ligand selected. J Immunol. 2000; 165:6156–6169. [PubMed: 11086049]

de Yebenes VG, Belver L, Pisano DG, Gonzalez S, Villasante A, Croce C, He L, Ramiro AR. miR-181b negatively regulates activation-induced cytidine deaminase in B cells. J Exp Med. 2008; 205:2199–2206. [PubMed: 18762567]

Dingjan GM, Maas A, Nawijn MC, Smit L, Voerman JS, Grosveld F, Hendriks RW. Severe B cell deficiency and disrupted splenic architecture in transgenic mice expressing the E41K mutated form of Bruton's tyrosine kinase. EMBO J. 1998; 17:5309–5320. [PubMed: 9736610]

Goodnow CC, Crosbie J, Adelstein S, Lavoie TB, Smith-Gill SJ, Brink RA, Pritchard-Briscoe H, Wotherspoon JS, Loblay RH, Raphael K, et al. Altered immunoglobulin expression and functional silencing of self-reactive B lymphocytes in transgenic mice. Nature. 1988; 334:676–682. [PubMed: 3261841]

Grimaldi CM, Hicks R, Diamond B. B cell selection and susceptibility to autoimmunity. J Immunol. 2005; 174:1775–1781. [PubMed: 15699102]

Gu H, Tarlinton D, Muller W, Rajewsky K, Forster I. Most peripheral B cells in mice are ligand selected. J Exp Med. 1991; 173:1357–1371. [PubMed: 1903427]

Halcomb KE, Musuka S, Gutierrez T, Wright HL, Satterthwaite AB. Btk regulates localization, in vivo activation, and class switching of anti-DNA B cells. Mol Immunol. 2008; 46:233–241. [PubMed: 18849077]

Harfe BD, McManus MT, Mansfield JH, Hornstein E, Tabin CJ. The RNaseIII enzyme Dicer is required for morphogenesis but not patterning of the vertebrate limb. Proc Natl Acad Sci U S A. 2005; 102:10898–10903. [PubMed: 16040801]

Hartley SB, Crosbie J, Brink R, Kantor AB, Basten A, Goodnow CC. Elimination from peripheral lymphoid tissues of self-reactive B lymphocytes recognizing membrane-bound antigens. Nature. 1991; 353:765–769. [PubMed: 1944535]

Hayakawa K, Hardy RR, Honda M, Herzenberg LA, Steinberg AD, Herzenberg LA. Ly-1 B cells: functionally distinct lymphocytes that secrete IgM autoantibodies. Proc Natl Acad Sci U S A. 1984; 81:2494–2498. [PubMed: 6609363]

Hobeika E, Thiemann S, Storch B, Jumaa H, Nielsen PJ, Pelanda R, Reth M. Testing gene function early in the B cell lineage in mb1-cre mice. Proc Natl Acad Sci U S A. 2006; 103:13789–13794. [PubMed: 16940357]

Ichiyoshi Y, Casali P. Analysis of the structural correlates for antibody polyreactivity by multiple reassortments of chimeric human immunoglobulin heavy and light chain V segments. J Exp Med. 1994; 180:885–895. [PubMed: 8064239]

Khan WN, Alt FW, Gerstein RM, Malynn BA, Larsson I, Rathbun G, Davidson L, Muller S, Kantor AB, Herzenberg LA, et al. Defective B cell development and function in Btk-deficient mice. Immunity. 1995; 3:283–299. [PubMed: 7552994]

Kim VN, Han J, Siomi MC. Biogenesis of small RNAs in animals. Nat Rev Mol Cell Biol. 2009; 10:126–139. [PubMed: 19165215]

Koralov SB, Muljo SA, Galler GR, Krek A, Chakraborty T, Kanellopoulou C, Jensen K, Cobb BS, Merkenschlager M, Rajewsky N, Rajewsky K. Dicer ablation affects antibody diversity and cell survival in the B lymphocyte lineage. Cell. 2008; 132:860–874. [PubMed: 18329371]

Li Y, Li H, Weigert M. Autoreactive B cells in the marginal zone that express dual receptors. J Exp Med. 2002; 195:181–188. [PubMed: 11805145]

Maas A, Dingjan GM, Grosveld F, Hendriks RW. Early arrest in B cell development in transgenic mice that express the E41K Bruton's tyrosine kinase mutant under the control of the CD19 promoter region. J Immunol. 1999; 162:6526–6533. [PubMed: 10352268]

Martin F, Kearney JF. Positive selection from newly formed to marginal zone B cells depends on the rate of clonal production, CD19, and btk. Immunity. 2000; 12:39–49. [PubMed: 10661404]

Martin F, Kearney JF. Marginal-zone B cells. Nat Rev Immunol. 2002; 2:323–335. [PubMed: 12033738]

Martin F, Oliver AM, Kearney JF. Marginal zone and B1 B cells unite in the early response against T-independent blood-borne particulate antigens. Immunity. 2001; 14:617–629. [PubMed: 11371363]

Martinez J, Busslinger M. Life beyond cleavage: the case of Ago2 and hematopoiesis. Genes Dev. 2007; 21:1983–1988. [PubMed: 17699747]

Meffre E, Casellas R, Nussenzweig MC. Antibody regulation of B cell development. Nat Immunol. 2000; 1:379–385. [PubMed: 11062496]

Meffre E, Wardemann H. B-cell tolerance checkpoints in health and autoimmunity. Curr Opin Immunol. 2008; 20:632–638. [PubMed: 18848883]

Nemazee DA, Burki K. Clonal deletion of B lymphocytes in a transgenic mouse bearing anti-MHC class I antibody genes. Nature. 1989; 337:562–566. [PubMed: 2783762]

Ng YS, Wardemann H, Chelnis J, Cunningham-Rundles C, Meffre E. Bruton's tyrosine kinase is essential for human B cell tolerance. J Exp Med. 2004; 200:927–934. [PubMed: 15466623]

Pillai S, Cariappa A. The follicular versus marginal zone B lymphocyte cell fate decision. Nat Rev Immunol. 2009; 9:767–777. [PubMed: 19855403]

Rickert RC, Roes J, Rajewsky K. B lymphocyte-specific, Cre-mediated mutagenesis in mice. Nucleic Acids Res. 1997; 25:1317–1318. [PubMed: 9092650]

Satterthwaite AB, Cheroutre H, Khan WN, Sideras P, Witte ON. Btk dosage determines sensitivity to B cell antigen receptor cross-linking. Proc Natl Acad Sci U S A. 1997; 94:13152–13157. [PubMed: 9371815]

Schmidt-Supprian M, Rajewsky K. Vagaries of conditional gene targeting. Nat Immunol. 2007; 8:665–668. [PubMed: 17579640]

Shlomchik MJ. Sites and stages of autoreactive B cell activation and regulation. Immunity. 2008; 28:18–28. [PubMed: 18199415]

Su TT, Guo B, Wei B, Braun J, Rawlings DJ. Signaling in transitional type 2 B cells is critical for peripheral B-cell development. Immunol Rev. 2004; 197:161–178. [PubMed: 14962194]

Wardemann H, Nussenzweig MC. B-cell self-tolerance in humans. Adv Immunol. 2007; 95:83–110. [PubMed: 17869611]

Wardemann H, Yurasov S, Schaefer A, Young JW, Meffre E, Nussenzweig MC. Predominant autoantibody production by early human B cell precursors. Science. 2003; 301:1374–1377. [PubMed: 12920303]

Whitacre CC. Sex differences in autoimmune disease. Nat Immunol. 2001; 2:777–780. [PubMed: 11526384]

Xiao C, Rajewsky K. MicroRNA control in the immune system: basic principles. Cell. 2009; 136:26–36. [PubMed: 19135886]

Europe PMC Funders Author Manuscripts

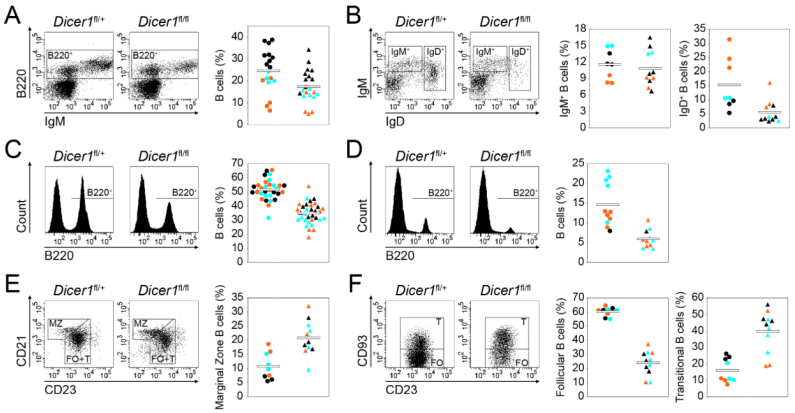

Figure 1. Total peripheral B cells are reduced and MZ and T subsets are overrepresented in the absence of Dicer

Phenotypic analysis of bone marrow (A and B), spleen (C, E and F) and lymph nodes (D) from CD19-Cre$^{ki/+}$Dicer$^{fl/+}$ and CD19-Cre$^{ki/+}$Dicer$^{fl/fl}$ mice. Cell suspensions were stained with the indicated antibodies and analysed by flow cytometry. Representative FACS analyses are shown on the left for total cells (A, C and D), B220^{+}-gated cells (B and E) or B220^{+}CD23^{bright}-gated cells (F). Graphs on the right show the frequency of the indicated subsets in individual mice analysed as follows, (A) B220^{+} bone marrow B cells (n=18-21, p=0.01); (B) IgM^{+}IgD$^{−}$ immature B (n=8-11, p=0.62) and IgD^{+} recirculating B cells (n=8-11, p<0.01); (C) B220^{+} spleen B cells (n=31-33, p<0.01); (D) B220^{+} lymph node cells (n=11, p<0.01); (E) CD21^{bright}CD23^{+} marginal zone (MZ) (n=9-11, p<0.01) and (F) CD21^{+}CD23^{bright}CD93$^{−}$ follicular (FO) (n=9-11, p<0.01) and CD21^{+}CD23^{bright}CD93^{+} transitional (T) cells (n=9-11, p<0.01) within total spleen B cells. Circles represent CD19-Cre$^{ki/+}$Dicer$^{fl/+}$ mice and triangles represent CD19-Cre$^{ki/+}$Dicer$^{fl/fl}$ mice. Color code represents mouse age (black, <10 weeks old; blue, 10 to 20 weeks old and orange, >20 weeks old). Mean values are shown as horizontal bars. See also Figure S1 and Table S1.

Europe PMC Funders Author Manuscripts

Europe PMC Funders Author Manuscripts

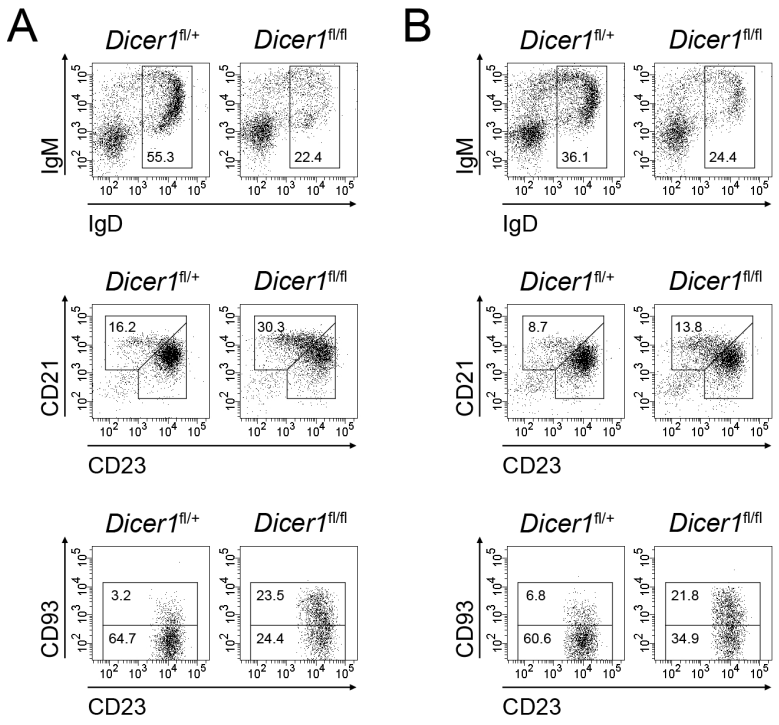

Figure 2. Dicer deficient cells in mixed chimeras show a reduction in total peripheral B cell generation and an overrepresentation of MZ and T subsets

Phenotypic analysis of bone marrow and spleen from lethally irradiated mice 12 weeks after bone marrow transfer with 100% CD45.2$^+$ CD19-Cre$^{ki/+}$Dicer$^{fl/+}$ or 100% CD45.2$^+$ CD19-Cre$^{ki/+}$Dicer$^{fl/fl}$ cells (A) and 1:1 mixtures of bone marrow cells from CD45.2$^+$ CD19-Cre$^{ki/+}$Dicer$^{fl/+}$ or CD45.2$^+$ CD19-Cre$^{ki/+}$Dicer$^{fl/fl}$ mice with bone marrow cells from CD45.1$^+$ wild type mice (B). Representative FACS analyses for the indicated markers are shown for B220$^+$-gated CD45.2$^+$ bone marrow cells (top histograms), B220$^+$-gated CD45.2$^+$ spleen cells (middle histograms) and B220$^+$CD23^{bright}-gated CD45.2$^+$ spleen cells (bottom histograms). Numbers in the gates show the percentage mean within CD45.2$^+$B220$^+$ cells of the following populations: top histograms, IgD$^+$ recirculating B cells (A: n=3, p<0.01; B: n=4, p<0.01); middle histograms, CD21^{bright}CD23$^+$ marginal zone B cells (A: n=3, p<0.01; B: n=4, p=0.03); bottom histograms, CD21$^+$CD23^{bright}CD93$^-$ follicular B cells (A: n=3, p<0.01; B: n=4, p<0.01) and CD21$^+$CD23^{bright}CD93$^+$ transitional B cells (A: n=3, p<0.01; B: n=4, p<0.01). Total numbers, means and standard deviations of the indicated cell subsets in the mixed chimeras are shown in Table S2. See also Figure S2.

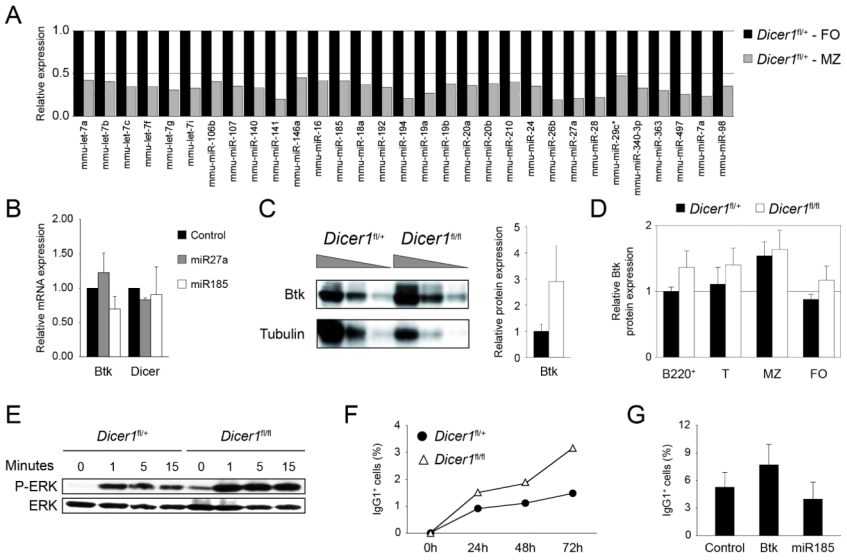

Figure 3. microRNA analysis of FO and MZ B cells and BCR signalling alterations in Dicer deficient cells

(A) microRNA profiling of FO and MZ subsets of CD19-Cre$^{ki/+}$Dicer$^{fl/+}$ mice. CD21^{+}CD23^{bright} follicular (FO) and CD21^{bright}CD23^{+} marginal zone (MZ) B cells were separated by cell sorting from CD19-Cre$^{ki/+}$Dicer$^{fl/+}$ spleens. RNA was isolated, labelled, and hybridized on Agilent microRNA arrays. Differentially expressed microRNAs in MZ (grey bars) *vs* FO (black bars) cells (see Methods) are shown ($p<0.1$). Bars represent fluorescence intensity normalized to FO cells (mean values of 3 independent experiments). (B) Differentially expressed microRNAs (shown in A) were subjected to target prediction analysis of genes potentially involved in MZ *vs* FO cell differentiation and/or maintenance. miR185 was predicted to target *Btk* by all three miRNA target prediction softwares used (MiRanda, TargetScan and miRBase). Control, miR185 and miR27a (not predicted to target *Btk*) retroviral vectors were transduced into primary B cells from wild type spleens in the presence of LPS and IL4. Two days after transduction RNA was isolated and *Btk* levels were measured by real-time RT-PCR (control *vs* miR185: n=4, $p<0.01$). Dicer mRNA levels from the same samples are shown as a negative control (control *vs* miR185: n=4, $p=0.73$). Bars represent mRNA levels after normalization to GAPDH expression and relative to control-transduced cells. Standard deviations are shown. (C) Btk protein level is increased in spleen B cells of Dicer deficient mice. 2-fold serial dilutions of total lysates from CD19-Cre$^{ki/+}$Dicer$^{fl/+}$ and CD19-Cre$^{ki/+}$Dicer$^{fl/fl}$ spleen B cells were analysed by Western blotting with anti-Btk and anti-tubulin antibodies. Densitometric quantification is shown on the right, black bar represents CD19-Cre$^{ki/+}$Dicer$^{fl/+}$ mice and white bar represents CD19-Cre$^{ki/+}$Dicer$^{fl/fl}$ mice (n=2, $p<0.01$). (D) Btk protein expression in B cell subsets. Spleen cell suspensions from CD19-Cre$^{ki/+}$Dicer$^{fl/+}$ (black bars) and CD19-Cre$^{ki/+}$Dicer$^{fl/fl}$ mice (white bars) were stained with anti-B220, anti-CD21, anti-CD23 and anti-CD93, intracellular stained with anti-Btk antibody and analysed by flow cytometry. Mean fluorescence in the indicated subsets was normalized to CD19-Cre$^{ki/+}$Dicer$^{fl/+}$ cell fluorescence in total B220^{+} cells (B220^{+}: n=8-10, $p<0.01$; T: n=8-10, $p=0.02$; MZ: n=8-10, $p=0.41$; FO: n=8-10, $p<0.01$). (E) Increased phospho-ERK levels in CD19-Cre$^{ki/+}$Dicer$^{fl/fl}$ cells. CD19-Cre$^{ki/+}$Dicer$^{fl/+}$ and CD19-Cre$^{ki/+}$Dicer$^{fl/fl}$ spleen B cells were stimulated with anti-IgM and total lysate from 1x10^{6} cells was loaded per lane for analyzing by Western blotting anti-phospho-ERK and anti-ERK protein levels. Time after stimulation is indicated over each lane. (F) Increased class switching in Dicer deficient cells upon stimulation with anti-IgM. Spleen B cells from CD19-Cre$^{ki/+}$Dicer$^{fl/+}$ (filled circles) and CD19-Cre$^{ki/+}$Dicer$^{fl/fl}$ mice

(triangles) were isolated and cultured in the presence of anti-IgM and IL4. The efficiency of class switch recombination to IgG1 was analysed by flow cytometry at the indicated time points (n=3). (G) Btk and miR185 gain-of-function analysis. Wild type spleen B cells were transduced with Btk, miR185 or empty vectors in the presence of anti-IgM and IL4. The efficiency of class switching to IgG1 was analysed by flow cytometry 96 hours after transduction. Bars represent the percentage of $IgG1^+$ cells within transduced GFP^+ cells. Standard deviations from three independent experiments are shown (n=3, p=0.03). See also Figure S3.

Europe PMC Funders Author Manuscripts

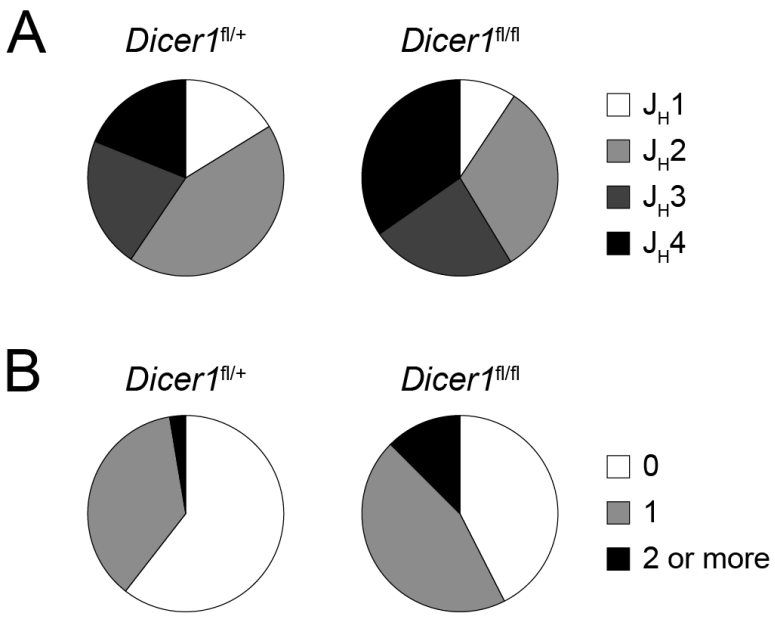

Figure 4. CD19-Cre$^{ki/+}$Dicer$^{fl/fl}$ B cells express a skewed Ig repertoire

Analysis of the expressed IgH repertoire in control and Dicer deficient B cells. B cells were isolated from CD19-Cre$^{ki/+}$Dicer$^{fl/+}$ and CD19-Cre$^{ki/+}$Dicer$^{fl/fl}$ spleens by immunomagnetic depletion. RNA was extracted, retrotranscribed and PCR-amplified with oligonuclotides specific for VHJ558 or VH7183 in combination with a Cμ oligonucleotide. PCR products were cloned, sequenced and analysed using IgBLAST software. Sectors represent the contribution of J_H segments (A) (n=74-75, $p<0.01$) and of sequences containing 0, 1 or >=2 R+K residues at CDR3 (B) (n=74-75, p=0.03) for CD19-Cre$^{ki/+}$Dicer$^{fl/+}$ and CD19-Cre$^{ki/+}$Dicer$^{fl/fl}$ B cells. Results were pooled from 4 independent animals of each genotype. Complete sequence analysis is shown in Table S3.

Europe PMC Funders Author Manuscripts

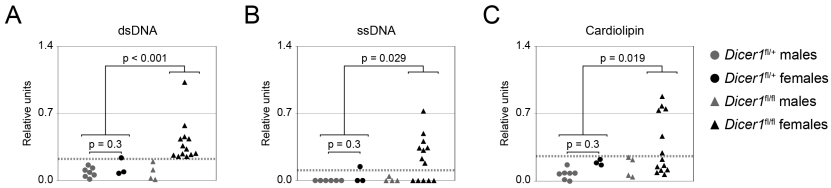

Figure 5. CD19-Cre$^{ki/+}$Dicer$^{fl/fl}$ mice have high serum titers of autoreactive antibodies

Analysis of serum Ig titers against self-antigens. Serum from 40-60 week old CD19-Cre$^{ki/+}$Dicer$^{fl/+}$ (circles) and CD19-Cre$^{ki/+}$Dicer$^{fl/fl}$ (triangles) animals was collected and reactivity against dsDNA (A), ssDNA (B) and cardiolipin (C) was assessed by ELISA. The results are represented as relative colorimetric units. Background signal from RAG knock-out mouse serum was substracted and values were normalized to the signal obtained from MRL$^{lpr/lpr}$ mouse serum. For clarity, results obtained from males (grey) and females (black) are represented separately. A threshold for autoreactive antibody titers was established by adding two standard deviations to the mean value of the titers detected in the control CD19-Cre$^{ki/+}$Dicer$^{fl/+}$ mice (shown as a grey dotted line). P values (Fisher's exact test) between the indicated groups are shown (n=9-17). See also Figure S4.

Europe PMC Funders Author Manuscripts

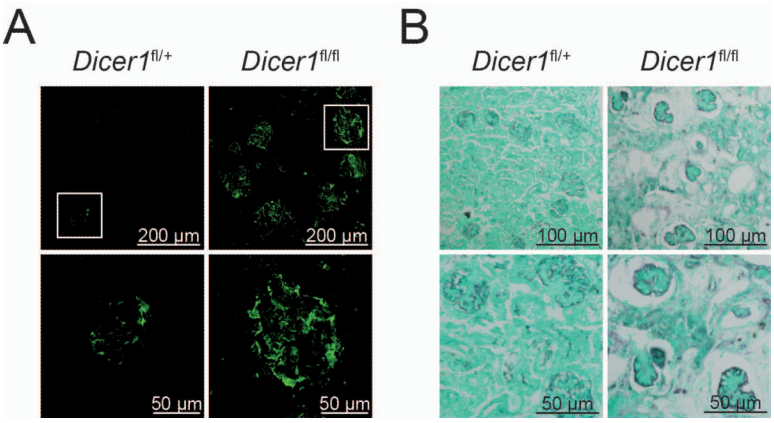

Figure 6. CD19-Cre$^{ki/+}$Dicer$^{fl/fl}$ females display autoimmune features

(A) Immunocomplexes in kidneys from Dicer deficient females. Kidney sections from 40-60 week old CD19-Cre$^{ki/+}$Dicer$^{fl/+}$ and CD19-Cre$^{ki/+}$Dicer$^{fl/fl}$ animals were stained with anti-IgG antibodies. Representative immunofluorescence glomerular stainings are shown at two different magnifications. Scale bars are indicated. (B) Kidney damage in CD19Cre$^{ki/+}$Dicer$^{fl/fl}$ mice. Formalin-fixed kidney sections from CD19Cre$^{ki/+}$Dicer$^{fl/+}$ and CD19Cre$^{ki/+}$Dicer$^{fl/fl}$ aged mice were subjected to Silver-PAS staining. Scale bars are shown. See also Figure S5.

Europe PMC Funders Author Manuscripts